

TIME-LINEARISED TRANSONIC SMALL DISTURBANCE CODE INCLUDING ENTROPY AND VORTICITY EFFECTS

Eddie Ly and Jiro Nakamichi
National Aerospace Laboratory of Japan (NAL)
Structures and Materials Research Center
Aeroelasticity Group, Tokyo 181-0015, Japan

Keywords: *ADI, entropy, shock, time-linearised, transonic, TSD equation, vorticity*

Abstract

The effect of small perturbations on steady transonic small-disturbance flowfield is studied. A time-linearised time-domain solution method that includes the shock motion effects via a shock jump correction procedure is presented. This correctly accounts for the small-amplitude shock motions due to small unsteady changes in the aerofoil boundary condition. The method also includes the shock-generated entropy and vorticity effects. Steady and first harmonic pressure distributions for NACA 0003 and NACA 0012 aerofoils are computed and compared with those obtained from the NAL's Euler code.

1 Introduction

Transonic flows are characterised by the presence of adjacent regions of subsonic and supersonic flow, usually accompanied by shock waves. In the past, there has been much activity in the development of computational methods for the analysis of time-linearised transonic flows. This activity was motivated by the need to supplement expensive and time consuming wind tunnel tests with an affordable, fast and reliable alternative.

This paper presents a solution method for computing time-linearised solution to the general-frequency transonic small disturbance (TSD) equation subject to non-reflecting farfield boundary conditions [13]. The advantages of the TSD formulation, particularly for aeroelas-

tic computations, are the relatively low computational cost and the simplicity of the gridding and geometry preprocessing. Two modifications are introduced into the inviscid TSD theory and existing potential code TranFlow2D (Transonic Flow 2D) to improve the accuracy of time-linearised solution. TranFlow2D is a suite of Fortran 90 codes capable of computing inviscid non-linear steady and unsteady, and time-linearised frequency-domain and time-domain solutions. A *Mathematica* package is also developed to assist the preprocessing (grid generator) and post-processing processes for the TranFlow2D code. First modification is the inclusion of the shock-generated entropy and vorticity effects to enhance the capability of TranFlow2D code in simulating flowfields with strong shocks. The second modification involves a procedure the first author refers to as the 'shock jump correction procedure' that allows one to include the effects of shock wave motion by 'correcting' the unsteady component of the time-linearised solution behind the shock. Previously time-linearised equation was solved in the frequency domain by numerous researchers, including the earliest by Traci, Albano and Farr Jr. [17], Hounjet and Schippers [15], Hounjet [10], and most recently, Greco, Lan and Lim [8], utilising a variety of computational methods of different levels of complexity, where shock motion was neglected. However, Fung, Yu and Seebass [5] were able to compute the time-linearised time-domain solution including shock motion effects, but their theory is based on the

low-frequency TSD equation, hence applications will be restricted to low-frequency flows.

Here the unsteady flow is treated as a small perturbation about the nonlinear steady flowfield, which results in a coupled problem for the steady and first-order unsteady reduced potentials. The steady problem is governed by the steady TSD equation [5, 13, 17], and shock-generated entropy and vorticity effects are incorporated. The first-order unsteady equation is linear, locally of mixed elliptic/hyperbolic type depending upon the nature of the steady-state solution, and solved in conjunction with the shock jump correction procedure. In the closure, comparisons of computed results for NACA 0003 aerofoil with a harmonically oscillating flap, and NACA 0012 aerofoil pitching harmonically about quarter-chord point, with those obtained from the NAL's Euler code will be made and discussed.

2 General-Frequency TSD Equation and Boundary Conditions

The unsteady, isentropic and inviscid flow over a thin aerofoil is assumed to be governed by the general-frequency TSD equation [6, 11], which may be written in conservation law form,

$$\frac{\partial}{\partial t} [\phi_t + 2\phi_x] + \frac{\partial}{\partial x} \left[\frac{1}{2}(\gamma + 1)W^2 \right] - \frac{\partial}{\partial z} [M_\infty^{-2}\phi_z] = 0, \quad (1)$$

where

$$W = \frac{1 - M_\infty^2}{M_\infty^2(\gamma + 1)} - \frac{\partial \phi}{\partial x}. \quad (2)$$

In the above and subsequent equations, $\phi_x = \partial\phi/\partial x$, (x, z) represents a dimensionless rectangular cartesian coordinate system with the coordinates based on an aerofoil chord length ℓ as the characteristic lengthscale, t : the dimensionless time variable based on the reciprocal of angular frequency ω , ϕ : the reduced potential based on the freestream fluid speed U_∞ times ℓ , M_∞ : the freestream Mach number, and γ : the ratio of specific heats (about 1.4 for ambient air). Equation (1) is locally of elliptic/hyperbolic type representing local subsonic/supersonic flow when W

is positive/negative, and its solution contains discontinuous jumps that approximate shock waves.

Non-reflecting boundary conditions, derived from the theory of wave propagation, are employed at the far-field computational boundaries, and Kutta condition is satisfied in the wake region behind the aerofoil. The flow tangency boundary condition is imposed on a flat mean surface (approximation to the aerofoil) in terms of aerofoil slopes, where the upper/lower side is defined by $z = h^\pm(x, t)$. The unbounded physical domain around an aerofoil is truncated at some finite distance. Non-reflecting far-field boundary conditions are imposed and serve to simulate the disturbances that propagate outward from the aerofoil to infinity. This allows the solution to propagate through the artificial computational boundaries as if there are no boundaries present. Consequently, the far-field boundaries can be moved closer to the aerofoil, and offer greater freedom in tradeoffs among grid density, accuracy and computational cost. The boundary conditions [6] imposed upon the flowfield are depicted in Figure 1. In this figure $\Delta_{z=0} f$ represents the jump in quantity f across the wake surface.

Any shock wave that exists in the flowfield must satisfy the shock jump condition derived from the conservation law form of Equation (1),

$$\langle \phi_t + 2\phi_x \rangle \langle \phi_x \rangle \frac{d\Lambda}{dt} + (\gamma + 1)\bar{W} \langle \phi_x \rangle^2 + M_\infty^{-2} \langle \phi_z \rangle^2 = 0, \quad (3)$$

where Λ and $d\Lambda/dt$ denote the instantaneous position and speed of the shock wave, respectively, \bar{W} is the average W value across the shock and $\langle \phi_x \rangle$ is the jump in ϕ_x across the shock (downstream minus upstream). The shock angle θ_{sw} , relative to the positive z -axis, is

$$\theta_{sw} = -\langle \phi_z \rangle / \langle \phi_x \rangle. \quad (4)$$

3 Time-Linearised Formulation

We treated the unsteady flow as a small perturbation about the nonlinear steady flowfield [13], which resulted in a coupled flow problem for the

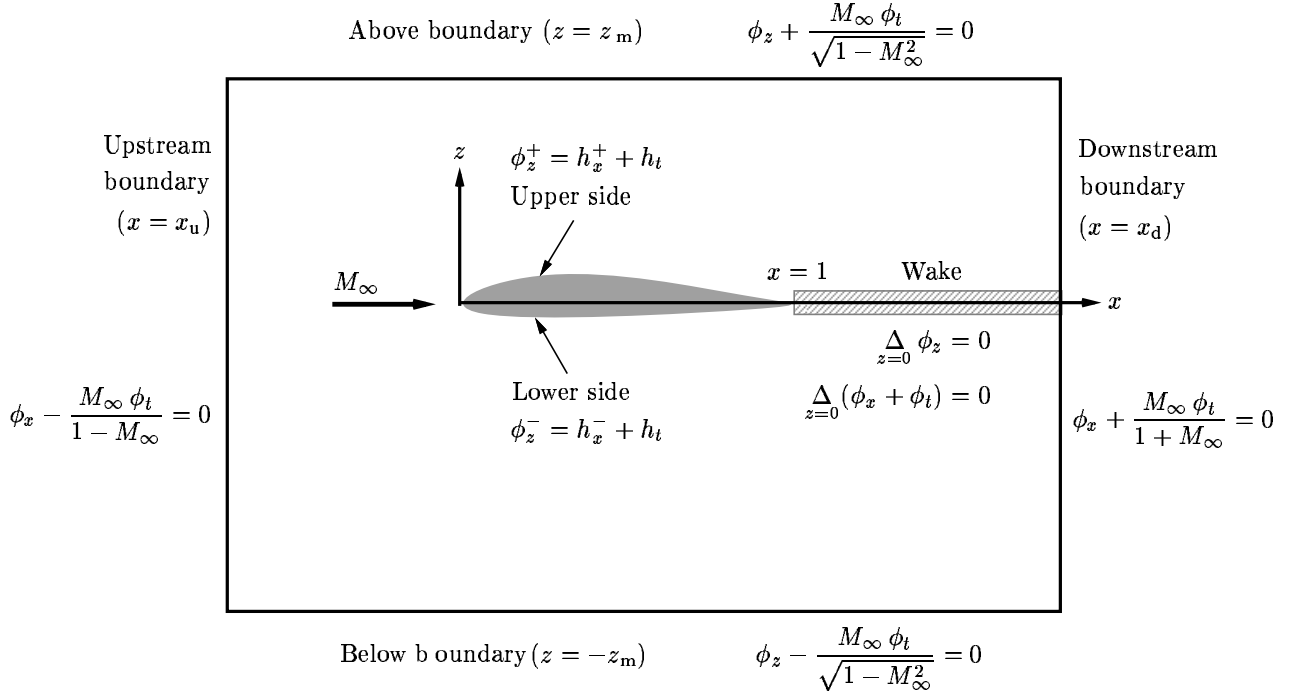


Fig. 1 Boundary conditions for two-dimensional transonic flow computations.

steady and first-order unsteady reduced potentials. The main dimensionless parameter governing the unsteady flow is the reduced frequency or Strouhal number, $k = \omega \ell / U_\infty$. The disturbance is assumed small [5, 16], so that the aerofoil motion and reduced potential can be respectively time-linearised as, to first-order approximations,

$$h^\pm(x, t) = h_s^\pm(x) + h_u(x, t), \quad (5)$$

$$\phi(x, z, t) = \phi_s(x, z) + \phi_u(x, z, t), \quad (6)$$

where subscripts s and u are used to identify the steady and unsteady components of a time-linearised quantity. In approximation (5), the aerofoil thickness effect is included in the steady flow analysis, whereas the unsteady analysis is performed for an aerofoil of vanishing thickness, but submerged in a steady reduced potential field.

To facilitate the use of high grid point density around the aerofoil, a smooth nonuniform computational mesh is constructed via an algebraic mapping process. In the mapping process, the far-field boundaries are kept independent of the aerofoil, and aligned with respect to the freestream direction, so that both the physical and computational domains are contained within

rectangular regions. The mapping functions are, in general terms,

$$\xi = \xi(x) \quad \text{and} \quad \zeta = \zeta(z), \quad (7)$$

where ξ and ζ are the dimensionless computational coordinates in the x - and z -direction.

Substituting (5) and (6) into Equation (1) with associated boundary conditions, and separating the steady and unsteady components, we found that ϕ_s satisfies (steady TSD equation),

$$\frac{\partial}{\partial \xi} \left[\frac{\gamma+1}{2\zeta_z} W_s^2 \right] - \frac{\partial}{\partial \zeta} \left[\frac{1}{M_\infty^2} \frac{\zeta_z}{\xi_x} \frac{\partial \phi_s}{\partial \zeta} \right] = 0, \quad (8)$$

where

$$W_s = \frac{1 - M_\infty^2}{M_\infty^2(\gamma+1)} - \xi_x \frac{\partial \phi_s}{\partial \xi}. \quad (9)$$

The required steady boundary conditions are those depicted in Figure 1 without the time-dependent terms and with ϕ_s replacing ϕ . While the unsteady component ϕ_u satisfies

$$\begin{aligned} \frac{\partial}{\partial t} \left[\frac{1}{\xi_x \zeta_z} \frac{\partial \phi_u}{\partial t} + \frac{2}{\zeta_z} \frac{\partial \phi_u}{\partial \xi} \right] - \frac{\partial}{\partial \xi} \left[(\gamma+1) \frac{\xi_x}{\zeta_z} W_s \frac{\partial \phi_u}{\partial \xi} \right] \\ - \frac{\partial}{\partial \zeta} \left[\frac{1}{M_\infty^2} \frac{\zeta_z}{\xi_x} \frac{\partial \phi_u}{\partial \zeta} \right] = 0, \end{aligned} \quad (10)$$

and the required boundary conditions are given in Figure 1 with ϕ_u replacing ϕ . Equation (10) is linear with respect to ϕ_u , and both (8) and (10) are of the same mixed elliptic/hyperbolic type as (1). Once ϕ is determined, the isentropic pressure coefficient C_p can be computed from

$$\begin{aligned} C_p &= C_{ps} + C_{pu} \\ &= -2 \left[\xi_x \frac{\partial \phi_s}{\partial \xi} + \xi_x \frac{\partial \phi_u}{\partial \xi} + \frac{\partial \phi_u}{\partial \tau} \right], \end{aligned} \quad (11)$$

where the first term on the right side corresponds to C_{ps} and the rest correspond to C_{pu} . The critical pressure coefficient C_p^* is defined by

$$C_p^* = \frac{-2(1 - M_\infty^2)}{M_\infty^2(\gamma + 1)}. \quad (12)$$

The solution for ϕ_s , which does not depend on ϕ_u , is solved independently, and is then used in the solution process for ϕ_u . This approach has the benefit that ϕ_s need not be regenerated for each unsteady boundary disturbance or reduced frequency of interest.

3.1 Inclusion of Shock-Generated Entropy and Vorticity Effects

The shock-generated entropy and vorticity effects, similar to those reported in references [4, 7, 9, 18] are incorporated into the steady analysis, so that flows with strong shocks can be simulated more accurately. Thence, Euler-like solutions are obtainable from the TSD theory.

Rotational effects become significant when strong shock waves exist in the flowfield, since vorticity is generated due to the entropy changes along the shock. Such effects are excluded in the conventional TSD theory because of the irrotationality assumption necessary for the existence of a velocity potential. Therefore, inclusion of the shock-generated entropy and vorticity effects is necessary when modelling such strong shocks. We replace the streamwise flux of Equation (8) by an alternative flux [1, 9, 18], and rewrite the equation with an artificial time derivative [11, 12, 13] appended (see Section 4),

$$\frac{\partial \phi_s}{\partial \tau} = \frac{\partial}{\partial \xi} \left[\frac{\gamma + 1}{2 \zeta_z} \widehat{W}_s^2 \right] - \frac{\partial}{\partial \zeta} \left[\frac{1}{M_\infty^2} \frac{\zeta_z}{\xi_x} \frac{\partial \phi_s}{\partial \zeta} \right], \quad (13)$$

where

$$\widehat{W}_s = \widehat{\vartheta} - \vartheta, \quad (14)$$

$$\widehat{\gamma} = \left[\frac{2 + (\gamma - 1)M_\infty^2}{(\gamma + 1)M_\infty^2} \right]^{\frac{1}{4}}, \quad (15)$$

$$\widehat{\vartheta} = \frac{1}{2}(\widehat{\gamma}^3 - 1/\widehat{\gamma}), \quad (16)$$

$$\vartheta = \frac{\widehat{\gamma}(1 + \widehat{\gamma}^2) \xi_x \frac{\partial \phi_s}{\partial \xi}}{1 + \widehat{\gamma}^2 + \xi_x \frac{\partial \phi_s}{\partial \xi}}, \quad (17)$$

where τ is an artificial time scale.

In the modification to include vorticity effects, the velocity vector is treated as a sum of potential and rotational components [2], and the rotational component assumed to exist only in the region downstream of the shock. Since entropy is constant for steady flow, and imposing that the shock curvature is negligibly small, the streamwise component of the fluid velocity vector ($u_s = 1 + \phi_x$) for grid points behind the shock is modified to

$$u_s = 1 + \xi_x \frac{\partial \phi_s}{\partial \xi} - \frac{1}{\gamma M_\infty^2} \frac{\Delta S}{R}, \quad (18)$$

where ΔS is an entropy jump a fluid particle experiences when it passes through a shock, and R is the specific gas constant. The entropy jump is a function of the normal Mach number upstream of the shock M_n (Rankine-Hugoniot shock jump relation),

$$\begin{aligned} \frac{\Delta S}{R} &= \frac{1}{\gamma - 1} \ln \left[\frac{2\gamma M_n^2 - \gamma + 1}{\gamma + 1} \right] \\ &\quad - \frac{\gamma}{\gamma - 1} \ln \left[\frac{(\gamma + 1)M_n^2}{2 + (\gamma - 1)M_n^2} \right]. \end{aligned} \quad (19)$$

This obviously requires the determination of the shock position before ΔS can be computed, which can be easily accomplished since the present algorithm uses a type-dependent differencing [3, 6] to capture shock waves (refer to Section 4 for details), and to properly treat local subsonic and supersonic regions. Consequently, the new steady equation will have a new streamwise flux defined by (13) and with u_s replaced by (18).

Table 1 Case studies.

Motion	Case	Aerofoil	M_∞	k	α_0	$\Delta\alpha$	δ_0	$\Delta\delta$	Figure
Flap oscillation	1	NACA 0003	0.93	0.125	0°	0°	0°	1°	2, 3
	2	NACA 0003	0.93	0.25	0°	0°	0°	1°	2, 3
Pitch oscillation	3	NACA 0012	0.84	0.25	0°	0.25°	0°	0°	4, 5
	4	NACA 0012	0.84	0.25	0°	0.5°	0°	0°	4, 5
	5	NACA 0012	0.8	0.25	1.25°	0.25°	0°	0°	6, 7

Note: α_0 = mean angle of attack
 δ_0 = mean flap angle

$\Delta\alpha$ = amplitude of pitch oscillation
 $\Delta\delta$ = amplitude of flap oscillation

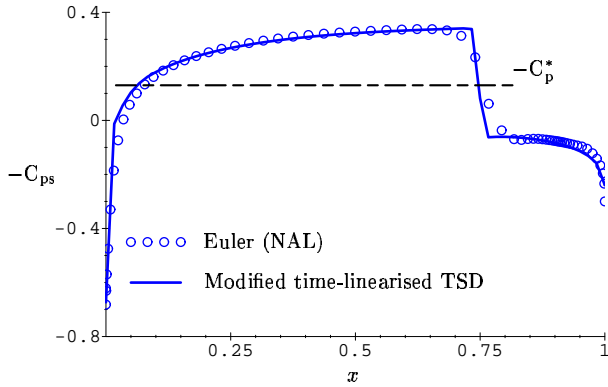


Fig. 2 Comparison of steady pressure distributions for the NACA 0003 aerofoil at $M_\infty = 0.93$ and $\delta_0 = 0^\circ$ ($x_h = 0.904$).

Modifications to the pressure formula and wake boundary conditions are also necessary. The modified pressure formula consists of an isentropic term (formula (11)) from the isentropic model, entropy related term and correction term due to vorticity. The wake boundary condition requires that the pressure be continuous across the wake, and since the pressure formula is now no longer containing just the isentropic term, the isentropic wake boundary condition must be modified to accommodate these changes. However, as discussed by Hafez and Lovell [9], the changes due to vorticity approximately cancel the changes due to entropy, and thus, the isentropic pressure formula still applies. Consequently, the wake boundary condition is identical to the original form as given in Figure 1 and formula (11) applied.

3.2 Inclusion of Shock Wave Motion Effects

In two-dimensional small perturbation transonic flows the shock waves that usually occur are nearly normal to the flow direction [16]. Therefore, we can assume that if the steady flowfield has a shock, then this shock may be approximated by a normal shock. We computed the shock motion in conjunction with the solution to Equation (10). The shock motion effect is incorporated into the computation by correcting the solution values behind the shock, such that the time-linearised form of Equation (3) is satisfied.

The shock motion is time-linearised [5, 13] as follows, to first-order approximation,

$$\Lambda(t) = \Lambda_s + \Lambda_u(t), \quad (20)$$

where $|\Lambda_u|$ is the amplitude of the time-linearised shock displacement. The reduced potential at the shock is expanded via a Taylor series expansion about $\xi = \xi(\Lambda_s)$ to give

$$\phi(\Lambda, \zeta, t) = \sum_{m=0}^{\infty} \frac{\Lambda_u^m}{m!} \left(\xi_x \frac{\partial}{\partial \xi} \right)^m \phi. \quad (21)$$

Substituting (6) and (20) into (21), and ensuring there is no circulation around the infinitesimal paths threading the shock front provides

$$\langle \phi_s(\Lambda_s, \zeta) \rangle = 0, \quad (22)$$

$$\langle \phi_u(\Lambda_s, \zeta, t) \rangle = -\Lambda_u \left\langle \xi_x \frac{\partial \phi_s}{\partial \xi} \right\rangle. \quad (23)$$

In addition to the above relations, the shock speed relation is required, so that Λ_u can be computed

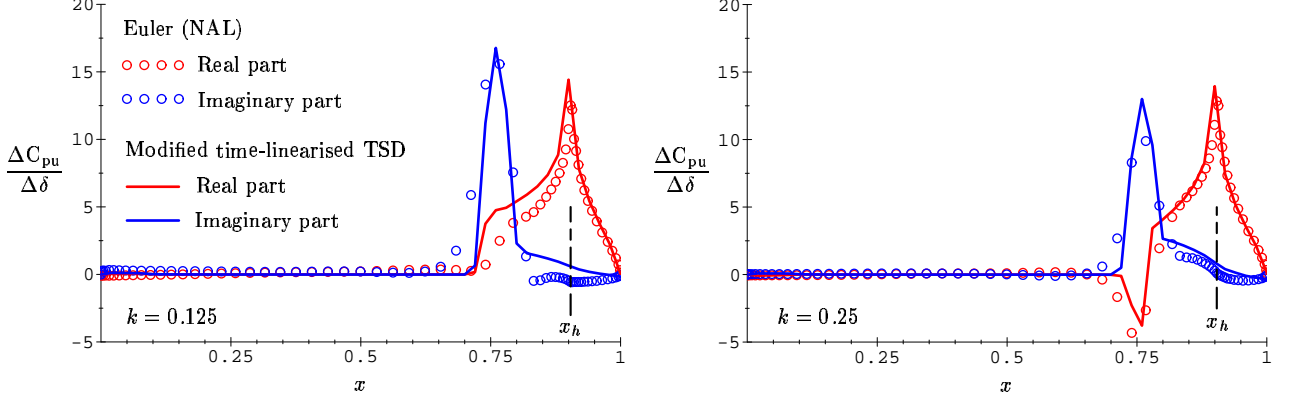


Fig. 3 Comparison of jump in first harmonic pressure across the NACA 0003 aerofoil with a harmonically oscillating 9.6% chord flap at $M_\infty = 0.93$, $k = 0.125$ (left plot) and 0.25 (right plot), $\delta_0 = 0^\circ$ ($x_h = 0.904$) and $\Delta\delta = 1^\circ$.

from the known values of ϕ_s and ϕ_u . Simplifying Equation (3) for normal shocks (i.e. imposing $\langle \phi_z \rangle = 0$), and making use of (6) and (20) leads to $\overline{W}_s = 0$ and the following shock speed relation,

$$\frac{d\Lambda_u}{dt} = \frac{\gamma + 1}{2} \overline{\xi_x} \frac{\partial \phi_u}{\partial \xi}. \quad (24)$$

Relation (24) is integrated at the shock foot at each time level of the solution process.

4 Numerical Solution Procedure

The numerical solution procedure involves applying the method of false transients [12] to solve Equation (8) for ϕ_s , and noniterative alternating directional implicit (ADI) method in conjunction with the shock jump correction procedure to solve Equation (10) for ϕ_u . In the method of false transients the artificial time derivative is evaluated by a general time difference rule, written in Padé form, and the spatial terms of the resulting equation is then approximately factorised. Time step cycling is employed as well to enhance the convergence rate of the scheme, see references [11, 12, 13] for more details.

The ADI method computes the solution by marching forward in time from its steady-state to subsequent time levels in a two-step process from time-level t_n to t_{n+1} , where $t_n = n\Delta t$ and Δt is the time step. Intermediate values at $t = t^*$ are computed at the midpoint of each time interval.

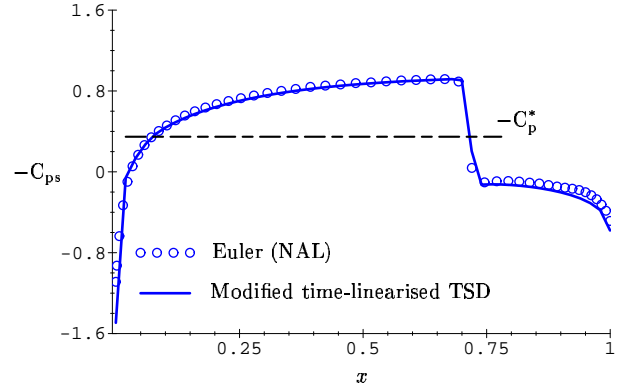


Fig. 4 Comparison of steady pressure distributions for the NACA 0012 aerofoil at $M_\infty = 0.84$ and $\alpha_0 = 0^\circ$.

We first write Equation (10) and boundary conditions at $t = t^*$, and evaluate $(\phi_u^*)_t$ by the trapezoidal rule and $(\phi_u^*)_{tt}$ by a non-standard second-order accurate forward differencing using solution from t_{n-2} to t_{n+1} levels. The ζ -derivative is averaged between t_n and t_{n+1} levels. Equation (10) is then split into two half equations with ϕ_u^* computed along the $\zeta = \text{constant}$ lines of the computational grid in the first half step, and then along the $\xi = \text{constant}$ lines in the second half step for ϕ_u^{n+1} . It is necessary to introduce boundary values for the intermediate solution (which will not be discussed here) that are compatible with the interior algorithms corresponding to the two half equations, so that a global truncation er-

ror of second-order in time can be attained. Relation (23) is also written at $t = t^*$ and differentiated with respect to time with (24) replacing $d\Lambda_u/dt$. The $\langle(\phi_u^*)_t\rangle$ term is evaluated by a first-order accurate forward differencing, and $\overline{\xi_x(\phi_u^*)_\xi}$ is estimated at $t = t_n$, thus resulting in the final finite difference scheme being globally second-order accurate in the spatial and time dimensions, except in the flow regions where shock motion occurs in which the time dimension is reduced to first-order accuracy.

In the finite difference schemes, the first ξ - and ζ -derivatives are differenced using standard second-order accurate upwind and central differencing, respectively, while second-order accurate Engquist-Osher type-dependent differencing [3, 6] is applied to the second ξ -derivatives. As the flow changes from subsonic to supersonic Engquist-Osher operators smoothly change from central differencing (elliptic region) to upwind differencing (hyperbolic region). This ensures a smooth transition from subsonic to supersonic flow. Hence, entropy violating decompression shocks will not develop. As the flow changes from supersonic to subsonic, Engquist-Osher operators change to an appropriate shock point operator [14], and for the computation of ϕ_u the shock jump correction is implemented. The correction procedure disregards the actual variation in ϕ_u , and thus, is only able to account for small-amplitude shock wave motions.

5 Results and Discussion

The effectiveness of the modifications to the modified TSD theory are determined by comparing present results with parallel Euler calculations for the cases tabulated in Table 1. All unsteady results become periodic within four cycles of oscillation.

5.1 NACA 0003 Aerofoil Results

The first two cases consider flows over an NACA 0003 aerofoil with a harmonically oscillating 9.6% chord flap (flap hinge at $x_h = 0.904$). The results are compared in Figures 2 and 3.

The steady pressure distribution corresponds reasonably well with the parallel Euler result as illustrated in Figure 2, except for the very small regions just upstream and downstream of the shock ($\Lambda_s = 0.747$) where the modified TSD theory gives a much sharper shock profile. However, the steady shock strength is well predicted. The jump in C_{ps} approximates the steady shock wave and where $C_{ps}/C_p^* > 1$ indicates locally steady supersonic point.

To assist in the comparisons of the unsteady results, approximating trace of the pressure responses in the form of a truncated Fourier series with only one harmonic is fitted to the results by a least squares procedure. The fitted parameters are then written in complex-valued form. Distributions of the real (in-phase) and imaginary (out-phase) parts of the jump in perturbation pressure coefficient across the aerofoil (i.e. $\Delta C_{pu} = C_{pu}^+ - C_{pu}^-$ where C_{pu}^+/C_{pu}^- is C_{pu} for the upper/lower side) per unit of flap deflection are shown Figure 3 for $k = 0.125$ and 0.25 . The positive peak of the real part is caused by the changes in aerofoil slopes across the flap hinge. While the peak of the imaginary part is due to the steady shock existence, leading to the observation that the shocks in the steady flowfield require corresponding shocks in the unsteady perturbation flowfield, which in effect result in harmonic changes in shock strength. Also noting that the comparison of the imaginary part behind the shock for Case 2 ($k = 0.25$) is much better than that of Case 1 ($k = 0.125$). The amplitude of shock displacement is proportional to $1/k$, and so, the flow region influenced by the shock motion effects for high-frequency flows is small, which suits the application of time-linearised methods, and hence, leads credence to the improvement of the imaginary part. Even though the modified TSD method slightly over predicted the pressure perturbation peaks, the comparison is good in general, since both methods give the same trend of pressure perturbation distributions along the aerofoil surfaces. Furthermore, all pressure peaks are correctly captured, particularly the negative peak appeared in the plot for $k = 0.25$ in Figure 3. The authors suspected

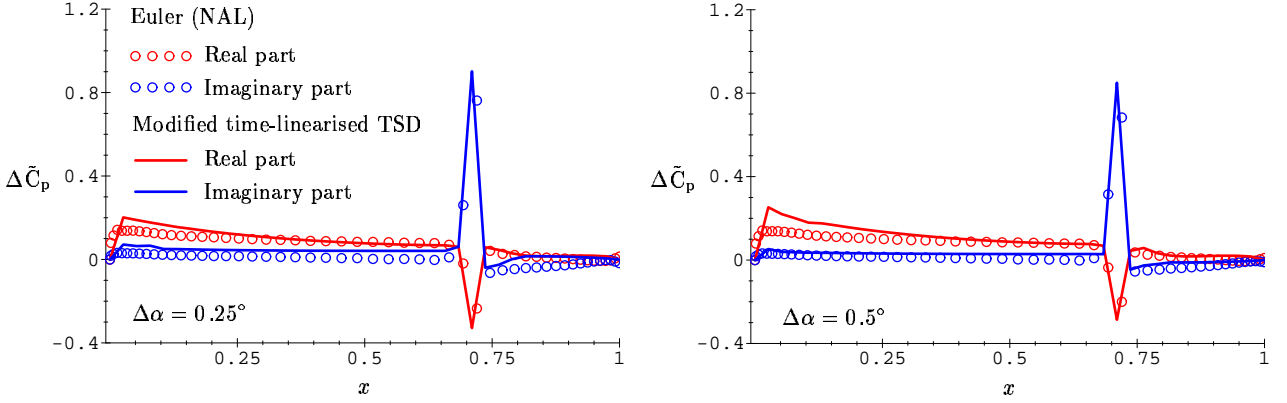


Fig. 5 Comparison of jump in first harmonic pressure across the NACA 0012 aerofoil pitching about quarter-chord point at $M_\infty = 0.84$, $k = 0.25$, $\alpha_0 = 0^\circ$, and $\Delta\alpha = 0.25^\circ$ (left plot) and 0.5° (right plot).

the small discrepancies in the comparisons are due to the amount of incorporated entropy being slightly different to the true value, and due to the fact that the unsteady flowfield is treated as a small perturbation about the steady flowfield instead of the true mean flowfield. However, the discrepancies in the shock region being small indicate that taking the steady flowfield and steady shock position to represent the mean flowfield and mean shock position, respectively, is reasonable. The mean shock position (Euler result) is determined to be about 75.6% chord, which is very close to the steady shock position (modified TSD result) of 74.7% chord, a difference in distance of less than 1% chord.

5.2 NACA 0012 Aerofoil Results

The next three cases are for flows over an NACA 0012 aerofoil pitching harmonically about quarter-chord point, and the results are compared in Figures 4 to 7. The steady part of Cases 3 and 4 is also studied by Fuglsang and Williams [4] and Whitlow Jr., Hafez and Osher [18], and the steady part of Case 5 is an AGARD test case for assessment of inviscid flow methods. The comparisons of the steady pressure distributions in Figures 4 and 6 are exceptional good, specifically in the accurate prediction of both the shock position and strength.

The perturbation pressure is extracted based

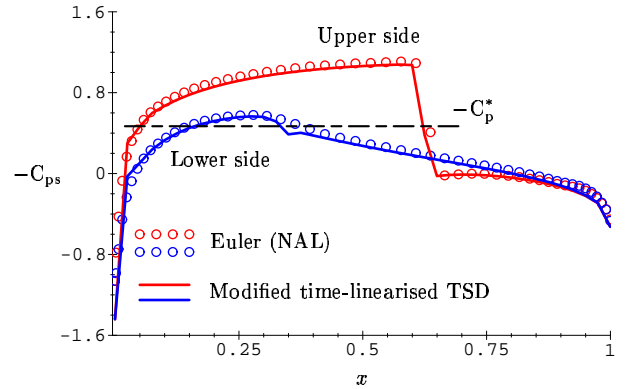


Fig. 6 Comparison of steady pressure distributions for the NACA 0012 aerofoil at $M_\infty = 0.8$ and $\alpha_0 = 1.25^\circ$.

on the following formula,

$$\Delta \tilde{C}_p = \frac{ik}{\pi \Delta\alpha} \oint C_p e^{ikt} dt, \quad (25)$$

where $\iota = \sqrt{-1}$ and $\Delta\alpha$ is in degree unit. There is no particular reason for using formula (25) to find $\Delta \tilde{C}_p$ here, which is not used for the NACA 0003 cases, except that the Euler results are provided by different group members. In general, the modified TSD method slightly over predicted the unsteady results as shown in Figures 5 and 7, but able to capture the trend of the pressure distributions determined by the Euler method, i.e. signs of the real and imaginary parts are the same. Since the NACA 0012 aerofoil has no flap or moveable lifting surfaces where the

aerofoil slopes change rapidly, the sharp pressure peaks shown by these plots are due to the shock, and again, well captured by the modified TSD method. The steady shock positions are very close to the mean values, thus increases the accuracy of the time-linearised results. The Euler method employs a body conformed dynamic grid system, in which a new grid is generated at each time level corresponding to the changes in aerofoil position. While the modified TSD method uses a stationary grid system with the flow tangency boundary condition imposed on a flat mean surface (approximation to the actual aerofoil) in terms of aerofoil slopes. Because of the different grid systems employed, the authors expected some discrepancies to occur near the aerofoil leading edge. The discrepancy occurs only for the real part of the pressure perturbation, and becomes large for large maximum angle of attack. For example, Figure 5 shows the discrepancy for Case 4 is larger than that of Case 3, since the angle of attack can reach upto 0.5° for Case 4 compares to 0.25° for Case 3. Similarly, much larger discrepancy occurs for Case 5 since the maximum angle of attack is 1.5° , see Figure 7. This observation is consistent with the expectation that the distribution of the real or in-phase part depends on the aerofoil profile and motion, since if comparing to Case 1 and 2 where only the flap that moves and 90.4% of the aerofoil is stationary, no such discrepancies occur near the leading edge. The small peaks that appeared in Figure 7 around 30% to 40% chord are generated by the vortex development in this region. Again, the modified TSD method captured such flow phenomenon remarkably well.

6 Concluding Remarks

An effective treatment of unsteady transonic flow with moving shock waves as a small perturbation about steady flowfield was presented. The solution method, in conjunction with the shock jump correction procedure and with inclusion of the shock-generated entropy and vorticity effects, has successfully produced accurate time-linearised time-domain solutions for tran-

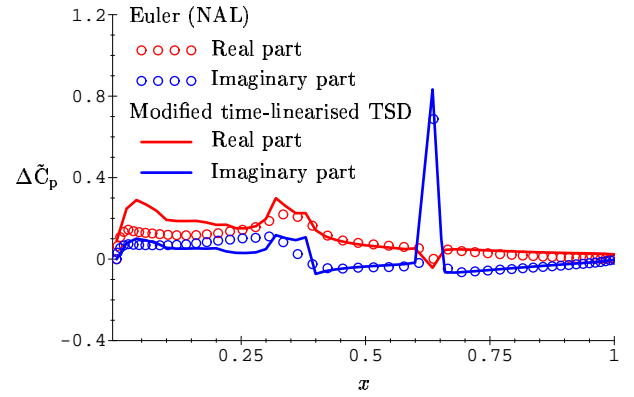


Fig. 7 Comparison of jump in first harmonic pressure across the NACA 0012 aerofoil pitching about quarter-chord point at $M_\infty = 0.8$, $k = 0.25$, $\alpha_0 = 1.25^\circ$ and $\Delta\alpha = 0.25^\circ$.

sonic flows with strong shocks. Consequently, Euler-like solutions for flows over representative aerofoil with a harmonically oscillating flap, and aerofoil pitching harmonically about quarter-chord point, both at high subsonic freestream Mach numbers, were obtained. These modifications to the inviscid TSD method leads to the development of a second version of the TransFlow2D code, a tool that provides the aeroelasticians with an affordable capability to perform intensive aeroelasticity computations.

Acknowledgments

This investigation was supported under the first author's Science and Technology Agency (STA/JSPS) Fellowship Program, commissioned by the Japan Science and Technology Corporation (JSTC) and Japan Society for the Promotion of Science (JSPS). The authors would like to thank Dr. John A. Gear of Mathematics Department of RMIT University, Melbourne, Australia, for proofreading this manuscript, and Dr. Masato Tamayama of NAL for providing the Euler solutions to the NACA 0003 aerofoil cases.

References

- [1] Batina J. Unsteady transonic small-disturbance theory including entropy and vorticity effects.

- Journal of Aircraft*, Vol. 26, No 6, pp 531–538, Jun. 1989.
- [2] Dang T and Chen L. An euler correction method for two- and three-dimensional transonic flows. AIAA Paper 87-0522, Jan. 1987.
- [3] Engquist B and Osher S. Stable and entropy satisfying approximations for transonic flow calculations. *Mathematics of Computation*, Vol. 34, No 149, pp 45–75, Jan. 1980.
- [4] Fuglsang D and Williams M. Non-isentropic unsteady transonic small disturbance theory. AIAA Paper 85-0600, Apr. 1985.
- [5] Fung K, Yu N, and Seebass R. Small unsteady perturbations in transonic flows. *AIAA Journal*, Vol. 16, No 8, pp 815–822, Aug. 1978.
- [6] Gear J, Ly E, and Phillips N. A time marching, type-dependent, finite difference algorithm for the modified transonic small disturbance equation. *Proc 21st International Council of the Aeronautical Sciences (ICAS) Congress*, Melbourne, Australia, 1998. Paper A98-31513.
- [7] Gibbons M, Whitlow Jr. W, and Williams M. Nonisentropic unsteady three dimensional small disturbance potential theory. AIAA Paper 86-0863, May 1986.
- [8] Greco P, Lan C, and Lim T. Frequency domain unsteady transonic aerodynamics for flutter and limit cycle oscillation prediction. AIAA Paper 97-0835, Jan. 1997.
- [9] Hafez M and Lovell D. Entropy and vorticity corrections for transonic flows. AIAA Paper 83-1926, Jul. 1983.
- [10] Hounjet M. NLR inviscid transonic unsteady loads prediction methods in aeroelasticity. Transonic Unsteady Aerodynamics and Aeroelasticity, AGARD-CP-507, pp 12.1-12.16, 1992.
- [11] Ly E. Improved approximate factorisation algorithm for the steady subsonic and transonic flow over an aircraft wing. *Proc 21st International Council of the Aeronautical Sciences (ICAS) Congress*, Melbourne, Australia, 1998. Paper A98-31699.
- [12] Ly E, Gear J, and Phillips N. Improved approximate factorisation algorithm. *Proc 8th Biennial Computational Techniques and Applications Conference (CTAC97)*, pp 393–400, Adelaide, Australia, 1997.
- [13] Ly E, Gear J, and Phillips N. Simulated shock motion using a time-linearised transonic code. *Proc 3rd Biennial Engineering Mathematics and Applications Conference (EMAC'98)*, pp 331–334, Adelaide, Australia, 1998.
- [14] Murman E. Analysis of embedded shock waves calculated by relaxation methods. *AIAA Journal*, Vol. 12, No 5, pp 626–633, May 1974.
- [15] Schippers H and Hounjet M. Two complementary approaches to transonic potential flow about oscillating airfoils. *Journal of Aircraft*, Vol. 25, No 5, pp 395–398, May 1988.
- [16] Tijdeman H. Investigations of the transonic flow around oscillating airfoils. Technical Report NLR TR 77090 U, National Aerospace Laboratory (NLR), Amsterdam, The Netherlands, Oct. 1977.
- [17] Traci R, Albano E, and Farr Jr. J. Perturbation method for transonic flows about oscillating airfoils. *AIAA Journal*, Vol. 14, No 9, pp 1258–1265, Sep. 1976.
- [18] Whitlow Jr. W, Hafez M, and Osher S. An entropy correction method for unsteady full potential flows with strong shocks. *Journal of Fluids and Structures*, Vol. 1, pp 401–414, 1987.